Sensors and Actuators B 258 (2018) 1287–1294

Contents lists available at ScienceDirect

Sensors and Actuators B: Chemical

journal homepage: www.elsevier.com/locate/snb

Long nanoneedle-electrode devices for extracellular and intracellular recording *in vivo*

Yoshihiro Kubota[a], Shota Yamagiwa[a], Hirohito Sawahata[a], Shinnosuke Idogawa[a], Shuhei Tsuruhara[a], Rika Numano[b,c], Kowa Koida[c,d], Makoto Ishida[a,c], Takeshi Kawano[a,*]

[a] *Department of Electrical and Electronic Information Engineering, Toyohashi University of Technology, Toyohashi, Aichi, Japan*
[b] *Department of Environmental and Life Sciences, Toyohashi University of Technology, Toyohashi, Aichi, Japan*
[c] *Electronics-Inspired Interdisciplinary Research Institute (EIIRIS), Toyohashi University of Technology, Toyohashi, Aichi, Japan*
[d] *Department of Computer and Science and Engineering, Toyohashi University of Technology, Toyohashi, Aichi, Japan*

ARTICLE INFO

Article history:
Received 16 September 2017
Received in revised form
16 November 2017
Accepted 24 November 2017
Available online 26 November 2017

Keywords:
Nanowire
Nanoelectrode
In vivo
Intracellular recording
Extracellular recording

ABSTRACT

Nanowire and nanotube-based nanoscale needle devices are powerful tools for intracellular applications, including electrical intracellular recording. However, the applications of these devices to thick biological tissues, such as brain slices or brain tissue *in vivo*, are limited due to the short length of conventional needles (<10 μm). In this study, we fabricated 200 μm- and 400 μm-long nanoscale-tipped microneedle-electrode (NTE) devices for *in vivo* applications. The fabricated NTEs penetrated tissue and could be used for both intracellular and extracellular recording, as demonstrated in mouse brain *in vivo*. Local field potentials (extracellular potentials) were recorded *via* the 200 μm-long device, whereas resting membrane potentials (intracellular potentials) were observed *via* the 400 μm-long device. Moreover, the NTE device could penetrate the dura mater. Thus, our long NTE device expands the application of nanodevices to intra- and extracellular recordings *in vivo*, which cannot be achieved using previously available nanoneedle devices, and should therefore contribute to a greater understanding of the nervous system.

1. Introduction

Nanoscale geometric devices, including nanowires and nanotubes, can enter the cell, enabling powerful intracellular applications such as electrical measurement, DNA transfer, and minimally invasive drug delivery [1–3]. In particular, intracellular electrophysiological recording has made significant contributions to our understanding of the nervous system, due to its large amplitude range of ~100 mV and the larger amount of neuronal information [excitatory and inhibitory postsynaptic potentials (EPSP and IPSP)] that can be obtained in comparison with extracellular recording. Previous studies have reported intracellular recording using single and multiple nanoscale devices [4–10]. The devices described in those studies had the ability to record cultured cells, but their applications to thick samples (*e.g.*, slices and *in vivo* brain tissues) were limited due to their short needle lengths (<10 μm).

One strategy for expanding the applicability of nanoscale devices to thick biological samples would be to employ longer nanowires that could penetrate tissue and reach the cell layer within it. We previously proposed a 120 μm-long high–aspect ratio vertical nanoscale-tipped microneedle-electrode (NTE), which has penetration capability due to its cone-like needle geometry. In addition, we demonstrated that this device can be used for *in vitro* intracellular recording in mouse muscle cells [11].

As a next step towards *in vivo* recording applications, longer NTE devices are necessary in order to reach cell layers in thick tissue [12] (*e.g.*, 160 and 210 μm for cortical layer 2/3 of mouse [13] and rat brain [14], respectively). Additionally, by employing an array of NTEs, one could perform intracellular signal recordings from multiple cells, as well as simultaneous intracellular and extracellular recordings *in vivo*. To realize these *in vivo* recording applications, we fabricated NTE devices with the needle lengths of 200 or 400 μm. We also explored the fabrication process of the NTE array device and device packages for *in vivo* applications, and

* Corresponding author at: Department of Electrical and Electronic Information Engineering, Toyohashi University of Technology, 1-1 Hibarigaoka Tempaku-cho, Toyohashi, Aichi, 441-8580, Japan.
E-mail address: kawano@ee.tut.ac.jp (T. Kawano).

https://doi.org/10.1016/j.snb.2017.11.152
0925-4005/

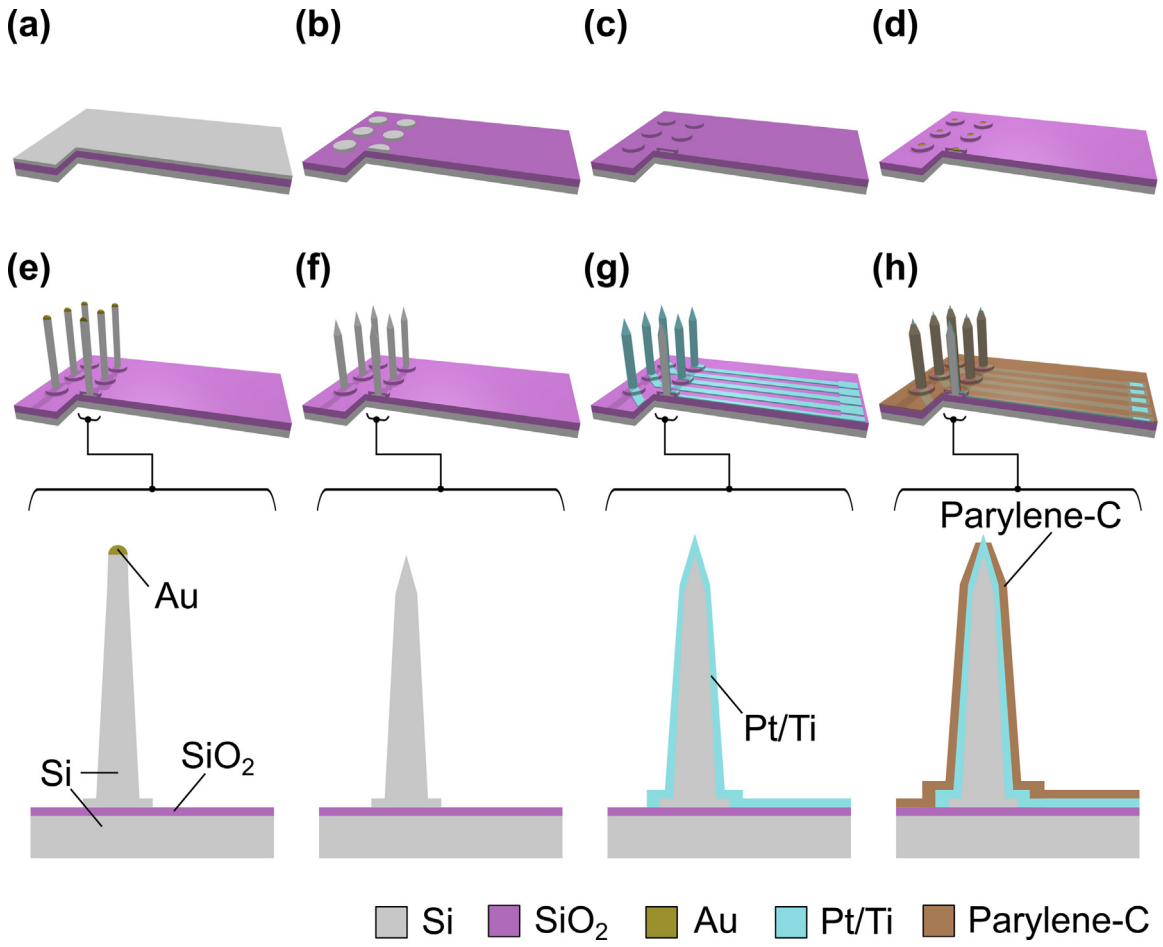

Fig. 1. Fabrication of an NTE array device. a) Silicon-on-insulator for the device substrate; b) formation of silicon islands with the (111)-top-silicon layer of the silicon-on-insulator; c) wet thermal oxidation of the silicon island; d) etching of silicon dioxide and catalytic-gold formation on the silicon island by evaporation and lift-off; e) VLS growth of silicon micro-scale needles; f) silicon chemical etching at the tip section of each silicon microneedle; g) metallization of the needle and device interconnection with platinum and titanium; and h) device encapsulation with parylene-C, and exposure of the platinum tip and the device bonding pad from the parylene-C layer by oxygen plasma.

demonstrated *in vivo* intracellular and extracellular recording using mouse brain tissue.

2. Methods

2.1. VLS growth of a silicon microneedle

Vapor-liquid-solid (VLS) growth of silicon with a catalytic-gold dot results in three-dimensional silicon needles. The fabrication process involves placing the substrate in a gas-source molecular-beam epitaxy (GS-MBE) chamber and conducting gold-catalyzed VLS growth of silicon to prepare individual silicon needles from the islands. The source of silicon gas was a mixture of 1% phosphine (PH_3) (diluted in 99% hydrogen) with 100% disilane (Si_2H_6) at a pressure of 10^{-3} Pa and a growth temperature of ~750 °C. The needle length was precisely controlled by maintaining a constant needle growth rate of 1.2 μm/min. Due to the vapor-phase deposition of silicon during VLS growth, poly-crystalline silicon was deposited over the substrate (silicon dioxide), which was removed by inductively coupled plasma reactive-ion etching (ICP-RIE).

2.2. Device fabrication

The fabrication process of the NTE array devices was based on a single-NTE device process reported in our previous work [11]. A silicon-on-insulator substrate [2-μm-thick (111)-top-silicon (*n*-type with a resistivity of <0.02 Ω cm)/4 μm-thick buried oxide layer/525 μm–thick (111)-silicon substrate (*n*-type with a resistivity of <0.02 Ω cm)] was used to fabricate the NTE array device (Fig. 1a). For electrical separations between the needle electrodes, silicon islands, which are silicon platforms for VLS-grown silicon needles, were patterned in the (111)-top-silicon layer (Fig. 1b). The islands were subsequently covered with a 1-μm-thick insulating layer of silicon dioxide by wet oxidation (Fig. 1c). Wet etching then exposed the silicon dioxide film where the catalytic gold used for VLS growth was placed by evaporation and lift-off (Fig. 1d). With a 200 nm–thick and 5 μm-diameter gold catalyst, a vertical silicon microneedle was formed by VLS growth of silicon at a growth rate of ~1.2 μm/min at ~750 °C ("2.1 VLS growth of a silicon microneedle", Fig. 1e). The length of the needle could be varied from 200 to 400 μm by altering the growth time (3 h for the 200 μm needle, and 6 h for the 400 μm needle). The base diameters of the 200 and 400 μm needles were 15 μm and 25 μm, respectively, whereas the tip diameters were the same (~3 μm) [15]. The microscale tip was then converted to nanoscale by silicon chemical etching, either with buffered HF following aqua regia treatment of the needle tip (Supplementary information, Fig. S1) or with $HF:HNO_3:H_2O$ solution (1:50:25) [16] (Fig. 1f). Metallization of both the silicon needle and the device interconnection were conducted by platinum sputtering with a binding layer of titanium (total thickness of platinum and titanium multilayer = 200 nm) (Fig. 1g). After metallization, the sidewall of the platinum-coated silicon needle and the device

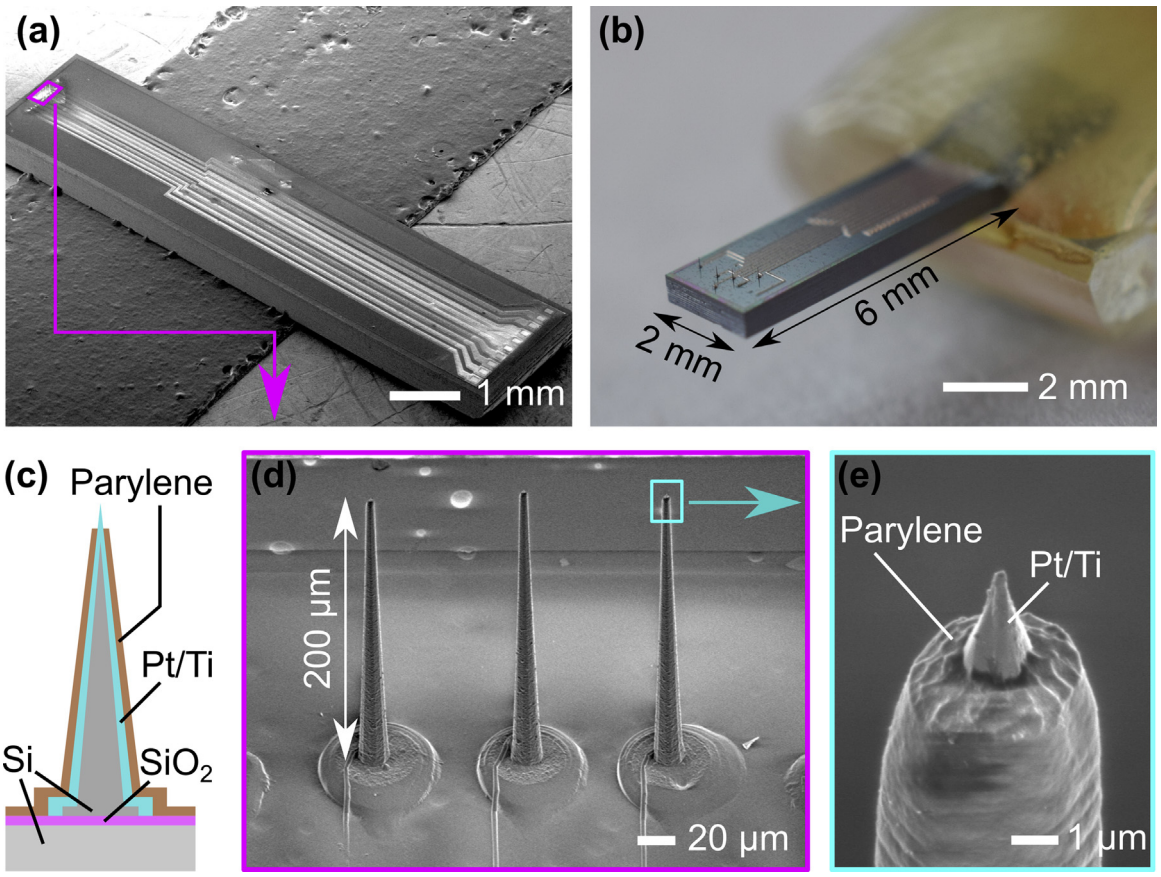

Fig. 2. Fabricated NTE array device. a) SEM image of a fabricated device die with dimensions of 2 mm × 8.75 mm. b) Photograph of a device package with a flexible printed circuit (FPC). c) Cross-sectional schematic of an NTE. d, e) SEM images of an array of three NTEs with a pitch of 80 μm, and the exposed platinum-nanotip section of an NTE. Height of the platinum-nanotip after exposure from the parylene shell is ~3.3 μm. Note that these SEM images are tilted at 45°.

interconnection were insulated by forming a <1 μm-thick biocompatible layer of parylene-C. The parylene-shelled needle was then covered with a spray-coated photoresist for subsequent exposure of the tip to oxygen plasma (Fig. 1h).

2.3. *Electrical characterizations*

The electrolyte/metal interfacial impedance of the electrode was measured in room-temperature phosphate-buffered saline (PBS) solution by applying a test sinusoidal wave with an amplitude of 100 mV_{p-p} at 1 Hz – 10 kHz *via* a counter-electrode (stainless). Impedance measurements were performed using impedance analyzer (Model 1260A Impedance/Gain-Phase Analyzer, Solartron Analytical, UK). The output/input (O/I) signal amplitude ratios of the recording system were analyzed in room-temperature 0.9% sodium chloride (NaCl) saline solution by applying sinusoidal wave test signals with an amplitude of ±100 mV at 1 Hz – 10 kHz *via* a counter-electrode (stainless). The output signals were amplified using a pre-amplifier (IX2 Dual Intracellular Preamplifier, Dagan, USA, input resistance = 10^{12} Ω) and a main amplifier.

2.4. In vivo *recordings*

The both extracellular and intracellular recording capability of the fabricated NTE devices was verified by measuring the local field potentials and the resting membrane potentials of mouse brain cells *in vivo*. A mouse (~25 g) was anesthetized by intraperitoneal injection of chlorprothixene (100 μl of 0.5% solution per 10 g body weight) and urethane (50 μl of 10% solution per 10 g body weight). Using the manipulator, the NTE device was placed on the exposed primary somatosensory cortex (S1B) of the mouse, and then penetrated the brain tissue; NTE penetration was confirmed by microscopy. All experimental procedures and animal care were approved by the animal experiments committee of Toyohashi University of Technology.

For extracellular recording, the fabricated NTE devices were packaged with a flexible printed circuit (FPC), which was connected to a recording amplifier (XC64, Tucker-Davis Technologies, USA, input impedance = 1×10^{14}). The signals recorded through the amplifier were acquired with a digital signal-processing module (RZ2, Tucker-Davis Technologies, USA). A vibrating stimulation system, which was driven by 2 ms duration pulse signals, was used for mechanical stimulation of the mouse's whiskers.

For intracellular recording, the fabricated NTE devices were packaged with a single-pin connector (1.4 mm diameter and 7.3 mm long), connected to a recording amplifier (IX2 Dual Intracellular Preamplifier, Dagan, USA; input resistance = 1×10^{12} Ω). Signals recorded through the amplifier were acquired with a digital signal-processing module (RZ2, Tucker-Davis Technologies, USA).

3. Results

3.1. *Fabricated device*

Fig. 2a and 2b show a SEM image of the fabricated device die and a picture of the package with a FPC. The die size of the fabricated device was 2 mm × 8.75 mm, suitable for *in vivo* application in mouse brain tissue. The yield of VLS growth of microneedles in each die was ~41%. Fig. 2c and d shows a cross-sectional schematic of a single NTE and a SEM image of a three-NTE array,

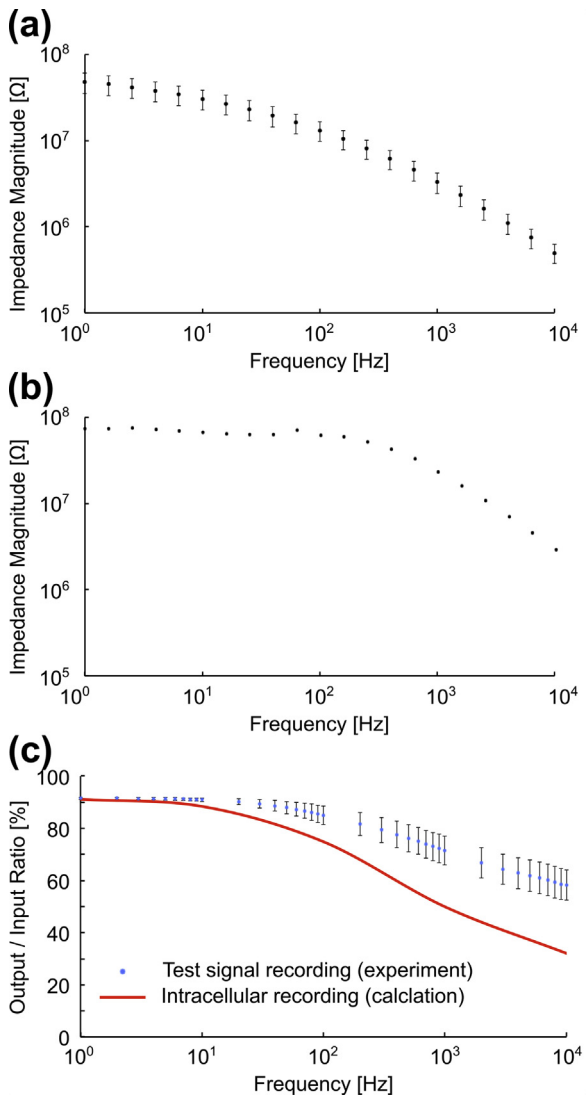

Fig. 3. Electrical characteristics of an NTE array device. a) Impedance magnitudes of NTEs measured in room-temperature PBS at frequencies of 1 Hz – 10 kHz. b) Impedance magnitudes between two interconnections in the array, measured in room-temperature PBS solution at frequencies of 1 Hz – 10 kHz. c) Output/input signal amplitude ratios taken from the test signal recordings. Test signals of ±100 mV sinusoidal waves at 1 Hz – 10 kHz were applied to the PBS solution. Averages and standard deviations of both impedance and O/I ratio were taken from eleven NTE samples.

respectively. The length of each NTE was 200 μm, whereas the pitch between the NTEs in the array ranged from 60 to 500 μm by photolithography-based alignment. The diameter and exposed height of each platinum nanotip were <300 nm and ~3.5 μm, respectively (Fig. 2e).

3.2. Electrical characteristics

We explored the electrical characteristics of the fabricated NTE array device, which has a small platinum recording area in the tip section (7.72 μm^2). Fig. 3a shows the magnitude of impedance taken from fabricated NTE devices immersed in PBS at room temperature. The NTEs exhibited the impedance magnitudes ranging from 496 kΩ to 48.4 MΩ (averages of 11 NTEs) at 1 Hz – 10 kHz, a frequency range corresponding to that of neuronal responses, including action potentials (1 kHz, impedance magnitude 3.32 MΩ). Because the measured impedances (Fig. 3a) include both the electrode's impedance and the interconnection-induced parasitic impedances, the electrode's impedance can be obtained by subtracting the interconnection's impedance [11]. Given the parasitic impedance (11 MΩ at 1 kHz, calculated value), the electrode's impedance at 1 kHz is 4.74 MΩ.

We also characterized electrical crosstalk between NTEs in the array (Fig. 3b). The crosstalk was measured in saline solution by applying the same test signal to the interconnections between two NTEs (platinum/titanium, ~8.26 mm in length, 30–60 μm in width, 200 nm in total thickness). The nearest-neighbor interconnections in the array were 30–60 μm apart (50–60 μm apart for the measured sample, Fig. S2). The impedance magnitudes measured at 1 Hz – 10 kHz ranged from 2.90 to 71.3 MΩ (22.9 MΩ at 1 kHz), higher than that of each NTE (496 kΩ to 48.4 MΩ at 1 Hz – 10 kHz, Fig. 3a).

To confirm amplitude attenuation of recorded neuronal signals associated with the fabricated NTE device and a recording system with a preamplifier (IX2 Dual Intracellular Preamplifier, Dagan, USA, input resistance = 10^{12} Ω), we also measured the O/I signal amplitude ratios of the NTE device with the recording system (Fig. 3c). The O/I ratios ranged from 58% to 92% (averages of 11 NTEs) at 1 Hz – 10 kHz (71% at 1 kHz for action potential recording). Due to the parasitic impedance of the device's interconnection, the O/I ratios decrease during actual neural recording [11]. In the test signal recording, the signal is measured through both the impedance of NTE's tip and the parasitic impedance of the device's interconnection (11 MΩ at 1 kHz, calculated value). However, in actual neuronal recording, the signal is measured through the NTE's tip, while the parasitic impedance is grounded. By considering the grounded parasitic impedance, the O/I ratios in actual neuronal recording can be obtained (red line in Fig. 3c, 49.9% at 1 kHz for action potential recording).

3.3. In vivo *extracellular recordings*

For chronic applications, it is important to minimize the risk of infection. One effective strategy to prevent infection is to leave the dura mater on the brain surface during electrode penetration. We were able to demonstrate NTE penetration without extraction of the dura mater. With a three-channel NTE linear array device, we confirmed that our NTE array could penetrate the dura mater, and we were simultaneously able to perform *in vivo* extracellular recording (Fig. 4). The barrel field region of S1B of an anesthetized mouse was exposed for NTE penetration (Fig. 4a and b). In these experiments, the length of each NTE in the array was 200 μm (Fig. 4c), allowing the NTE to punch through the dura mater and reach the cell layers (layer 2/3). The NTE array device then penetrated the S1B at a speed of ~50 μm/s (Fig. 4d and Movie S1).

Fig. 4e show spectrograms, waveforms, and power spectra recorded *via* the three-channel NTEs in the array (Chs. #3, #5, and #8). In this experiment, NTE Ch. #5 was positioned at the center of the S1B. The Ch. #3 and #8 NTEs were located 120 μm and 180 μm from the center (NTE Ch. #5), respectively. The acquired signals had different waveforms and power spectrums between the three NTE channels. These waveforms consisted of lower-frequency components in comparison with action potentials (~1 kHz), whereas signals in response to whisker stimulation had a latency of ~25 ms (black arrow in each waveform in Fig. 4e). Each power spectrum after sensory stimulation had several peaks in the frequency range of 40–50 Hz (Lower gamma, 'Lγ' in Fig. 4e) and 200–400 Hz (Fast oscillations, 'FO' in Fig. 4e). FO is a typical sensory response recorded from the somatosensory cortex [17]. Because of the frequency and latency of these signals, the recorded signals were considered to be somatosensory evoked potential (SEP) induced by the whisker stimulations [14].

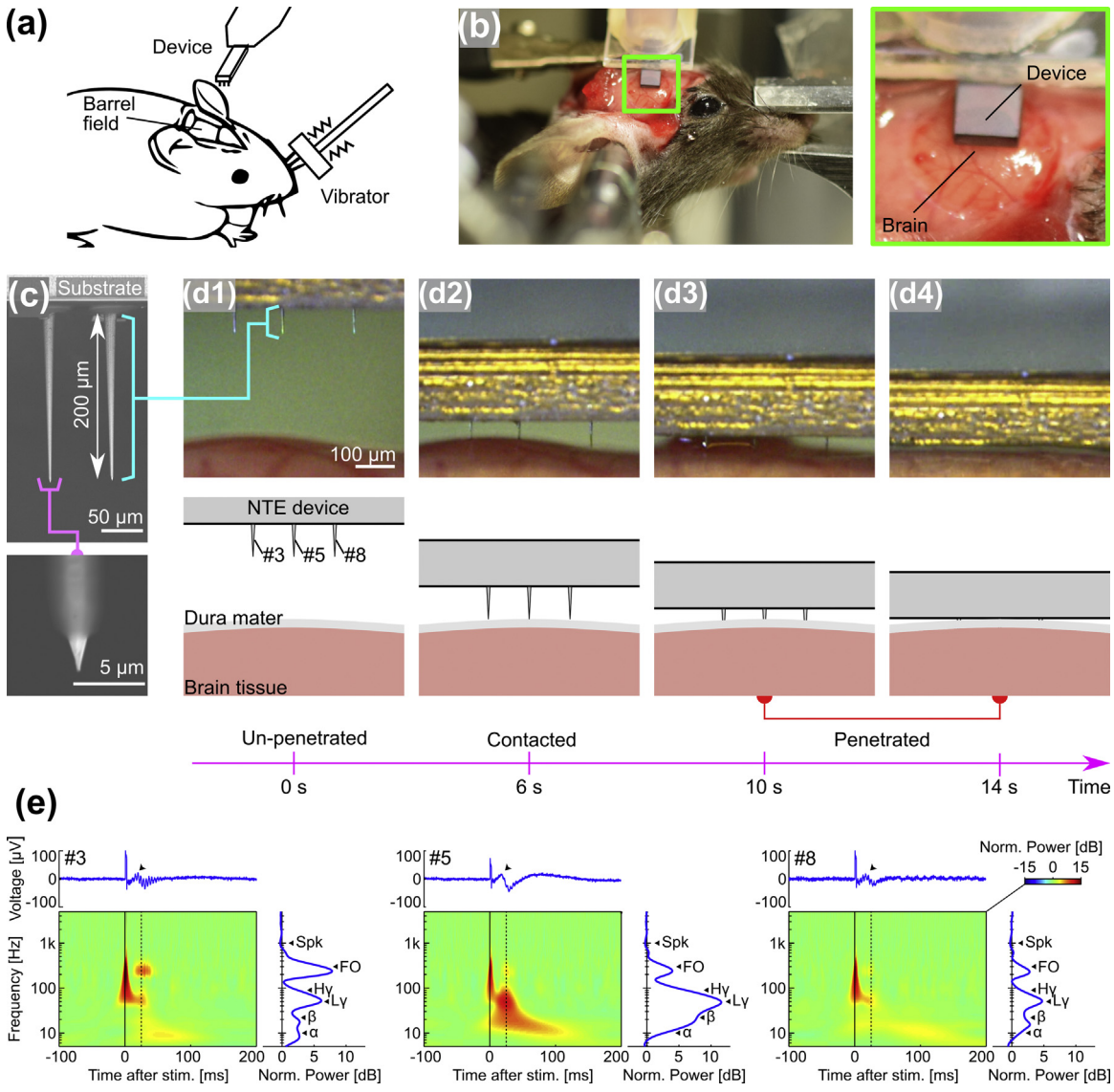

Fig. 4. *In vivo* extracellular recording from mouse primary somatosensory cortex (S1B). a, b) Schematic and photograph of the experimental setup. The NTE device was placed on the exposed S1B of the mouse, and then penetrated the brain tissue. c) SEM image of the NTE used in these experiments. The length of the NTE was 200 μm. d) NTE prior to penetration, in contact with the brain, or after penetration into the brain. NTE penetration was conducted through the dura mater. e) Spectrograms, waveforms, and power spectrum acquired *via* channel #3, #5, and #8 NTEs, respectively.
α, β, Lγ, Hγ, FO and Spk in each power spectra show center frequencies of alpha wave, beta wave, low-gamma wave, high-gamma wave, fast electrical oscillations, and spike (action potential), respectively. Each spectrogram is transformed by wavelet transformation (gabor, σ = 1). Note that waveforms were 5–100 Hz bandpass-filtered (first order Butterworth filter), and the large signal at 0 s is an artifact of stimulation.

3.4. In vivo *intracellular recordings*

To evaluate the intracellular recording capability of the fabricated NTE device, we performed NTE penetration using mouse brain tissue *in vivo*. Fig. 5a and b show the measurement system used in the intracellular recordings. We used 400 μm-long NTE devices (Fig. 5c), with the device mounted on an *xyz* manipulator. Using the manipulator, the NTE device was placed on the exposed S1B of the mouse, and then penetrated the brain tissue at a speed of 50 μm/s; NTE penetration was confirmed by microscopy (Fig. 5d and Movie S2).

During NTE penetration into brain tissue, four of eight trials with the same NTE device revealed potential changes: −92.2 mV for trial 1, −98.2 mV for trial 2, −89.1 mV for trial 3, and −52.9 mV for trial 4 [average, −81.3 ± 20 mV (mean ± SD)] (Fig. 5e). Each potential change was observed at a depth of ∼400 μm. Each resting membrane potential was calculated by subtracting the potential 500 ms after the abrupt change from the potential 500 ms before the one. After the abrupt change, the decreased potential remained until the NTE was moved upward. These potential changes were also observed with a glass pipette electrode with a tip diameter of ∼800 nm (Supplemental materials, Fig. S3). Potential changes were also observed in our previous study, in which an NTE device (impedance magnitudes of 1.2–2.3 MΩ at 1 kHz) penetrated mouse's tibial muscle cell *in vitro*, with potential changes of −19 to −35 mV [11]. We did not observe action potentials during the sensory stimulation. In addition, we observed no significant fractures of the needle itself, as confirmed by extraction of the needle from the tissue. These results indicated that the fabricated 400 μm-long NTE device could measure the resting membrane potentials of cells *in vivo*.

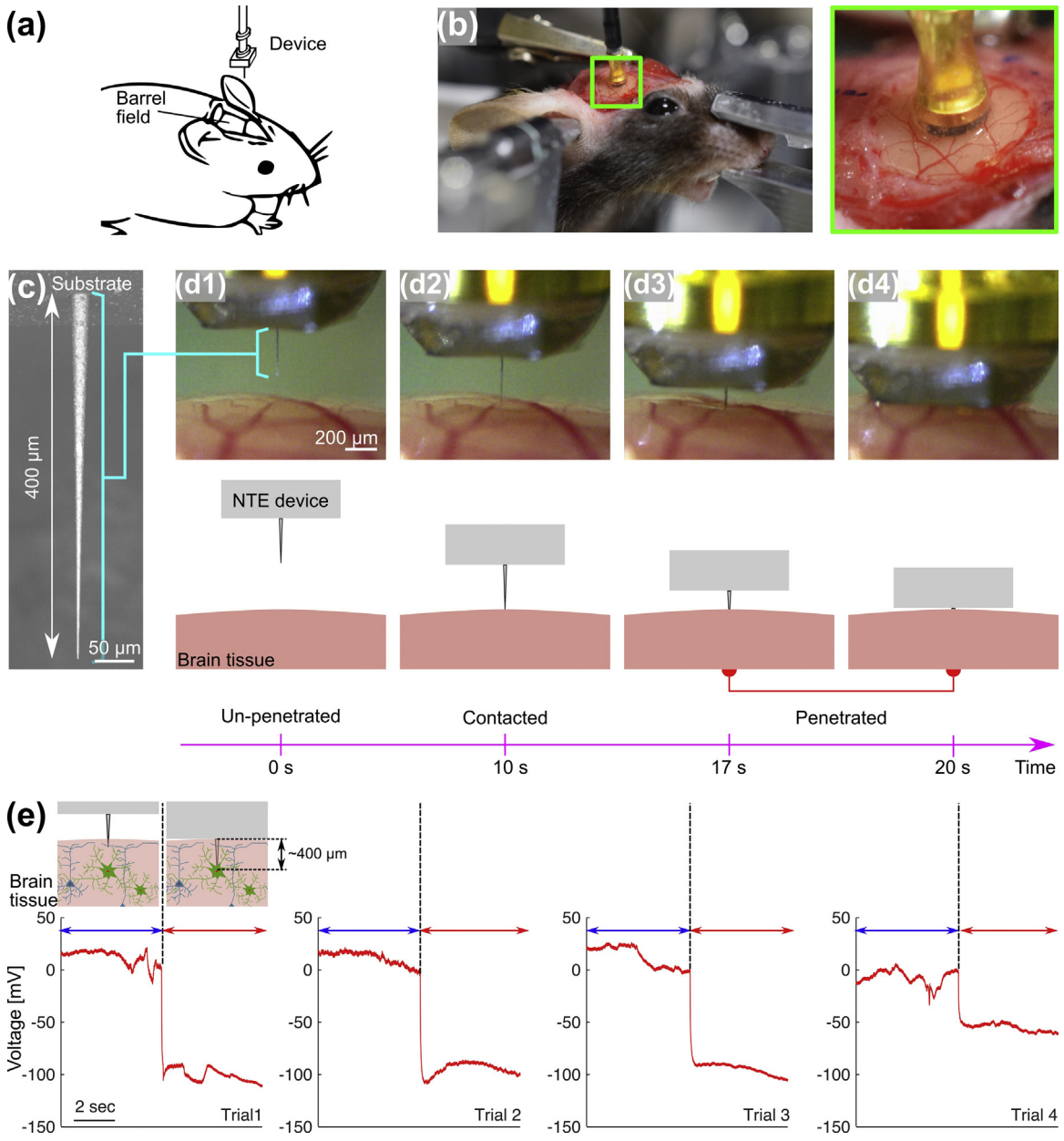

Fig. 5. *In vivo* neuronal intracellular recordings from primary somatosensory cortex (S1B) of a mouse. a, b) Schematic and photograph of the experimental setup. The NTE device was placed on the exposed S1B of an anesthetized mouse. c) SEM image of the NTE used in these experiments. The length of the NTE was 400 μm. d) NTE prior to penetration, in contact with the brain, or after penetration into the brain. NTE penetration was conducted in the absence of the dura mater. e) Waveforms taken from four trials of NTE penetrations.

4. Discussion

In this study, we fabricated nanoscale-tipped microneedle electrodes with lengths ranging from 200 to 400 μm, enabling us to reach cells in layers 2/3–4 of mouse cortex (~1 mm in thickness). For animals larger than mice, such as rat and monkey, longer needles will be necessary to approach the corresponding cell layers in brain tissue. In VLS growth, needle length can be controlled by adjusting growth time, with a growth ratio of 1.2 μm/min at 750 °C [18]; using this approach, we have grown needles up to ~2 mm long [14]. We have also reported a dissolvable material–based scaffold for the tissue penetration of such high aspect ratio silicon microneedles [19]. On the other hand, shorter NTEs (<200 μm) fabricated by decreasing the growth time can be applied to thinner biological samples, such as cultured cells or brain slices *in vitro*.

The NTEs had the ability to penetrate through the dura mater, as demonstrated by *in vivo* recording in mouse brain. This property is important in order to minimize the risk of brain infection, particularly in the chronic applications. Another advantage of our device is that it caused no significant deformation of brain tissue during NTE penetration. Tissue deformation causes physical stress to the tissue, and should therefore be minimized. Although we have not performed quantitative analysis of tissue deformation, these data will be reported in a future study, including an analysis of tissue damage and a comparison of deformation and damage using other needle-electrodes with different diameters.

The NTE exhibited reduced O/I signal amplitude ratios at >10 Hz due to the high impedance of the electrode [14]; the data were consistent with the results of the extracellular recordings, in which the recorded signals did not consist of high-frequency components of action potentials. Each needle electrode has a nanoscale plat-

inum tip with an area of 7.72 μm^2, with an impedance of 4.74 MΩ and an O/I signal amplitude ratio of 49.9% at 1 kHz. These electrical properties of the NTE attenuate the amplitudes of high-frequency components of recorded signals; consequently, no action potentials were recorded. To enable recording of action potentials, one way to decrease the electrode impedance would be to increase the area (height) of the needle tip section (>3.5 μm in height, >7.72 μm^2 in area) by lengthening the oxygen plasma process (Fig. 1h) [11]. However, an increased tip area would not be suitable for application to intracellular recordings. Another approach would be to use a low-impedance material instead of platinum, such as iridium oxide (IrOx) [20,21] or poly(3,4-ethylenedioxythiophene) (PEDOT) [22–25], without increasing the area of the nanotip section.

For *in vivo* intracellular recording from mouse brain tissue, we used 400 μm-long NTE devices. On the other hand, intracellular potentials could not be observed using 200 μm-long NTE devices, largely due to the low density of cells, including neurons and glia, in layers 1 and 2/3 of mouse cortex [26]. These results were consistent with preliminary tests using glass pipette electrodes, in which intracellular potentials were observed at depths ranging from 350 μm (layer 4) to 1050 μm (layer 6). Based on that, we used the 400 μm-long NTE devices for the intracellular recordings.

The 400-μm-long NTE device enabled measurement of the resting membrane potentials of cells. However, we did not observe action potentials of neuron with our NTE devices. In mouse brain tissue, the numbers of neurons and glia are comparable [27]. In our recordings, resting membrane potentials measured in three of four trials of the NTE penetration were −92.2 mV, −98.2 mV, and −89.1 mV, higher than neuron potential (−70 mV) but similar to that of glial cells [28]. This suggests that our NTE device penetrated either glial cells or neurons (silent neurons) and measured their resting membrane potentials. To achieve NTE penetration into neurons and recording of the action potentials, it is necessary to increase the probability of neuron penetration by increasing the number and density of the NTEs to levels resembling those of neurons in the tissue (neuronal densities in mouse tissue are $137{,}645 \pm 6410/mm^3$ for layer 2/3 and $181{,}362 \pm 6142/mm^3$ for layer 4 [29]).

During intracellular recordings, we observed potential fluctuations (Fig. 5e). The fluctuation is probably due to the material properties of the NTE's tip (platinum), because less fluctuation was observed in intracellular recordings using a glass pipette electrode (Supplemental materials, Fig. S3c). In the recording with the NTE, amplitude of the fluctuation before the abrupt change was relatively larger than that of after the one. One reason of the difference in fluctuation amplitude is probably due to that the NTE contacts cells or something during the downward manipulation of the NTE (before the abrupt change).

Although the NTEs could not record action potentials in either intracellular or extracellular recording, they could record both extracellular signals of local field potential and intracellular signals of resting membrane potential from mouse brain *in vivo*. Previously, we reported that VLS-grown platinum black tipped low impedance microneedle-electrodes (<500 kΩ at 1 kHz in saline) had the ability to record extracellular action potentials [14]. The electrode's low impedance increased the O/I signal amplitude to 97% at 1 kHz. Similar to extracellular action-potential recording, intracellular action-potential recording also requires the device to have a high O/I ratio, either due to lower impedance of the needle or high parasitic impedance of the device interconnection. In addition, an increase in the density of NTEs is necessary to increase the probability of neuron penetration. Therefore, by combining future device designs incorporating high O/I signal amplitude ratios and high-density arrays of electrodes, our NTE array device could be applied to extracellular and intracellular recording of action potentials. In addition, NTEs with high O/I signal amplitude ratios could record not only action potentials, but also excitatory and inhibitory postsynaptic potentials (EPSPs and IPSPs), providing fundamental insights into the properties of the brain and nervous system *in vivo*.

5. Conclusions

In this study, we developed long-nanoneedle electrode devices for *in vivo* recording applications. To enable electrode penetration into brain tissue *in vivo*, we fabricated 200 and 400-μm-long needles by silicon-microwire growth and subsequent nanotip formation. Such needles can also be assembled as arrays for multisite recording applications. We demonstrated the penetration and recording capabilities of the nanoneedle electrode devices in mouse brain *in vivo*. Although the nanoneedles were not able to record neuronal action potentials, we demonstrated their ability to record for the local field potentials and resting membrane potentials *in vivo*. Following refinement of the electrode's properties (*e.g.*, impedance), our long-nanoneedle electrode devices will enable intracellular recordings of action potentials from multiple neurons in brain tissue *in vivo*, as well as thick brain slices *in vitro*. Such recording applications, which cannot be realized by previously available nanoelectrode devices with needle lengths <10 μm, will contribute to a greater understanding of the brain and nervous system.

Acknowledgements

This work was supported by Grants-in-Aid for Scientific Research (A) (No. 25249047), (B) (No. 17H03250), for Young Scientists (A) (No. 26709024), on Innovative Areas (Research in a proposed research area) (15H05917), the PRESTO Program from JST, and Strategic Advancement of Multi-Purpose Ultra-Human Robot and Artificial Intelligence Technologies program from NEDO. Y.K. was supported by the Leading Graduate School Program R03 of MEXT. R.N. was supported by Takeda Science Foundation.

Appendix A. Supplementary data

Supplementary data associated with this article can be found, in the online version, at https://doi.org/10.1016/j.snb.2017.11.152.

References

[1] S.-W. Han, C. Nakamura, N. Kotobuki, I. Obataya, H. Ohgushi, T. Nagamune, J. Miyake, High-efficiency DNA injection into a single human mesenchymal stem cell using a nanoneedle and atomic force microscopy, Nanomedicine 4 (2008) 215–225.
[2] A.K. Shalek, J.T. Robinson, E.S. Karp, J.S. Lee, D.-R. Ahn, M.-H. Yoon, A. Sutton, M. Jorgolli, R.S. Gertner, T.S. Gujral, G. MacBeath, E.G. Yang, H. Park, Vertical silicon nanowires as a universal platform for delivering biomolecules into living cells, Proc. Natl. Acad. Sci. U. S. A. 107 (2010) 1870–1875.
[3] R. Singhal, Z. Orynbayeva, R.V. Kalyana Sundaram, J.J. Niu, S. Bhattacharyya, E.A. Vitol, M.G. Schrlau, E.S. Papazoglou, G. Friedman, Y. Gogotsi, Multifunctional carbon-nanotube cellular endoscopes, Nat. Nanotechnol. 6 (2011) 57–64.
[4] B. Tian, T. Cohen-Karni, Q. Qing, X. Duan, P. Xie, C.M. Lieber, Three-dimensional, flexible nanoscale field-effect transistors as localized bioprobes, Science 329 (2010) 830–834.
[5] X. Duan, R. Gao, P. Xie, T. Cohen-Karni, Q. Qing, H.S. Choe, B. Tian, X. Jiang, C.M. Lieber, Intracellular recordings of action potentials by an extracellular nanoscale field-effect transistor, Nat. Nanotechnol. 7 (2012) 174–179.
[6] R. Gao, S. Strehle, B. Tian, T. Cohen-Karni, P. Xie, X. Duan, Q. Qing, C.M. Lieber, Outside looking In: nanotube transistor intracellular sensors, Nano Lett. 12 (2012) 3329–3333.
[7] C. Xie, Z. Lin, L. Hanson, Y. Cui, B. Cui, Intracellular recording of action potentials by nanopillar electroporation, Nat. Nanotechnol. 29 (2012) 997–1003.
[8] J.T. Robinson, M. Jorgolli, A.K. Shalek, M.-H. Yoon, R.S. Gertner, H. Park, Vertical nanowire electrode arrays as a scalable platform for intracellular interfacing to neuronal circuits, Nat. Nanotechnol. 7 (2012) 180–184.

[9] Q. Qing, Z. Jiang, L. Xu, R. Gao, L.Q. Mai, C.M. Lieber, Free-standing kinked nanowire transistor probes for targeted intracellular recording in three dimensions, Nat. Nanotechnol. 9 (2014) 142–147.
[10] R. Liu, R. Chen, A.T. Elthakeb, S.H. Lee, S. Hinckley, M.L. Khraiche, J. Scott, D. Pre, Y. Hwang, A. Tanaka, Y.G. Ro, A.K. Matsushita, X. Dai, C. Soci, S. Biesmans, A. James, J. Nogan, K.L. Jungjohann, D.V. Pete, D.B. Webb, Y. Zou, A.G. Bang, S.A. Dayeh, High density individually addressable nanowire arrays record intracellular activity from primary rodent and human stem cell derived neurons, Nano Lett. 17 (2017) 2757–2764.
[11] Y. Kubota, H. Oi, H. Sawahata, A. Goryu, Y. Ando, R. Numano, M. Ishida, T. Kawano, Nanoscale-tipped high-aspect-ratio vertical microneedle electrodes for intracellular recordings, Small 12 (2016) 2846–2853.
[12] J. DeFelipe, The evolution of the brain, the human nature of cortical circuits, and intellectual creativity, Front. Neuroanat. 5 (2011).
[13] H. Sawahata, S. Yamagiwa, A. Moriya, T. Dong, H. Oi, Y. Ando, R. Numano, M. Ishida, K. Koida, T. Kawano, Single 5 μm diameter needle electrode block modules for unit recordings in vivo, Sci. Rep. 6 (2016) 35806.
[14] A. Fujishiro, H. Kaneko, T. Kawashima, M. Ishida, T. Kawano, In vivo neuronal action potential recordings via three-dimensional microscale needle-electrode arrays, Sci. Rep. 4 (2014) 4868.
[15] T. Kawano, Y. Kato, M. Futagawa, H. Takao, K. Sawada, M. Ishida, Fabrication and properties of ultrasmall Si wire arrays with circuits by vapor-liquid-solid growth, Sens. Actuators A Phys. 97–98 (2002) 709–715.
[16] A. Goryu, A. Ikedo, M. Ishida, T. Kawano, Nanoscale sharpening tips of vapor-liquid-solid grown silicon microwire arrays, Nanotechnology 21 (2010) 125302.
[17] M.S. Jones, D.S. Barth, A.M. Oswald, B. Doiron, J. Rinzel, A.D. Reyes, Effects of bicuculline methiodide on fast (>200 Hz) electrical oscillations in rat somatosensory cortex, J. Neurophysiol. 101 (2011) 6–1025.
[18] A. Ikedo, T. Kawashima, T. Kawano, M. Ishida, Vertically aligned silicon microwire arrays of various lengths by repeated selective vapor-liquid-solid growth of n-type silicon/n-type silicon, Appl. Phys. Lett. 95 (2009) 20–23.
[19] S. Yagi, S. Yamagiwa, Y. Kubota, H. Sawahata, R. Numano, T. Imashioya, H. Oi, M. Ishida, T. Kawano, Dissolvable base scaffolds allow tissue penetration of high-aspect-ratio flexible microneedles, Adv. Healthc. Mater. 4 (2015) 1949–1955.
[20] S. Yamagiwa, A. Fujishiro, H. Sawahata, R. Numano, M. Ishida, T. Kawano, Layer-by-layer assembled nanorough iridium-oxide/platinum-black for low-voltage microscale electrode neurostimulation, Sens. Actuators B Chem. 206 (2015) 205–211.
[21] S.F. Cogan, J. Ehrlich, T.D. Plante, A. Smirnov, D.B. Shire, M. Gingerich, J.F. Rizzo, Sputtered iridium oxide films for neural stimulation electrodes, J. Biomed. Mater. Res. Part B Appl. Biomater. 89 (2009) 353–361.
[22] S.J. Wilks, S.M. Richardson-Burns, J.L. Hendricks, D.C. Martin, K.J. Otto, Poly(3,4-ethylenedioxythiophene) as a micro-neural interface material for electrostimulation, Front. Neuroeng. 2 (2009) 1–8.
[23] D. Khodagholy, T. Doublet, M. Gurfinkel, P. Quilichini, E. Ismailova, P. Leleux, T. Herve, S. Sanaur, C. Bernard, G.G. Malliaras, Highly conformable conducting polymer electrodes for in vivo recordings, Adv. Mater. 23 (2011) 268–272.
[24] S. Venkatraman, J. Hendricks, Z.A. King, A.J. Sereno, S. Richardson-Burns, D. Martin, J.M. Carmena, In vitro and in vivo evaluation of PEDOT microelectrodes for neural stimulation and recording, IEEE Trans. Neural Syst. Rehabil. Eng. 19 (2011) 307–316.
[25] M.R. Abidian, D.C. Martin, Multifunctional nanobiomaterials for neural interfaces, Adv. Funct. Mater. 19 (2009) 573–585.
[26] J.Q. Ren, Y. Aika, C.W. Heizmann, T. Kosaka, Quantitative analysis of neurons and glial cells in the rat somatosensory cortex, with special reference to GABAergic neurons and parvalbumin-containing neurons, Exp. Brain Res. 92 (1992) 1–14.
[27] S. Herculano-Houzel, The glia/neuron ratio: how it varies uniformly across brain structures and species and what that means for brain physiology and evolution, Glia 62 (2014) 1377–1391.
[28] W. Meme, M. Vandecasteele, C. Giaume, L. Venance, Electrical coupling between hippocampal astrocytes in rat brain slices, Neurosci. Res. 63 (2009) 236–243.
[29] J. DeFelipe, L. Alonso-Nanclares, J.I. Arellano, Microstructure of the neocortex: comparative aspects, J. Neurophysiol. 31 (2003) 299–316.

Biographies

Yoshihiro Kubota completed his B.S. in 2013 and M.S. in 2015 in the Department of Electrical and Electronic Engineering, Toyohashi University of Technology, Japan. From 2016–2017, he was a visiting student in the Department of Mechanical Engineering, University of California, Berkeley, USA. He is pursuing his Ph.D. in the Department of Electrical and Electronic Engineering, Toyohashi University of Technology, Japan.

Shota Yamagiwa completed his M.S. in 2012 and Ph.D. in 2016 in the Department of Electrical and Electronic Engineering, Toyohashi University of Technology, Japan. He is currently working as a Postdoctoral Research Fellow in the Department of Electrical and Electronic Information Engineering, Toyohashi University of Technology, Japan.

Hirohito Sawahata was a Postdoctoral Research Fellow in the Graduate School of Medical and Dental Sciences, Niigata University, Japan, from 2009 to 2012. He completed his Ph.D. in the Graduate School of Science and Engineering, Yamagata University, Japan. From 2012–2013, he worked as an Assistant Professor at the Graduate School of Medical and Dental Sciences, Niigata University, Japan. Since 2013, he has been working as an Assistant Professor in the Department of Electrical and Electronic Information Engineering, Toyohashi University of Technology, Japan.

Shinnosuke Idogawa completed his B.S. in 2013 from the Department of Electrical and Electronic Engineering, Toyohashi University of Technology, Japan. He is pursuing his M.S. at the same institution.

Shuhei Tsuruhara is pursuing his B.S. in the Department of Electrical and Electronic Engineering, Toyohashi University of Technology, Japan.

Rika Numano completed her B.S. in 1996, M.S. in 1998, and Ph.D. in 2002, all in the Faculty of Technology, The University of Tokyo, Japan. From 2002–2005, she was a Postdoctoral Research Fellow (Japan Society for the Promotion of Science) at the Human Genome Center Institute of Medical Science, The University of Tokyo, Japan. From 2005–2006, she was a Postdoctoral Fellow (Japan Society for the Promotion of Science Postdoctoral fellowship for research abroad) in the Department of Molecular and Cell Biology, University of California, Berkeley, USA; from 2006 to 2007, a researcher in Cell Function Dynamics, RIKEN, Japan; from 2007 to 2009, a researcher in the ERATO Project, Japan Science and Technology Agency; and from 2009 to 2013, a tenure-track Associate Professor, Electronics-Inspired Interdisciplinary Research Institute (EIIRIS), Toyohashi University of Technology, Japan. Since 2013, she has worked as an Associate Professor in the Department of Environmental and Life Sciences, Toyohashi University of Technology, Japan.

Kowa Koida completed his Ph.D. at the Interdisciplinary Graduate School of Science and Engineering, Tokyo Institute of Technology, Japan, in 2000. From 2000–2007, he was a Postdoctoral Research Fellow at the National Institute for Physiological Sciences, Japan, and from 2007 to 2010 he continued his work there as an Assistant Professor. He is currently working as an Associate Professor, Department of Computer and Science and Engineering, Toyohashi University of Technology, Japan, and Electronics Inspired-Interdisciplinary Research Institute (EIIRIS) at the same institution.

Makoto Ishida completed his Ph.D. in Department of Electronics Engineering at Kyoto University, Japan, and worked as a Research Assistant, Department of Electric and Electronic Engineering, Toyohashi University of Technology, Japan. Starting in 1997, he worked as a Professor, Department of Electrical and Electronic Engineering, Toyohashi University of Technology, Japan. From 2008, he served as Vice President of Research Affairs, Director of Electronics-Inspired Interdisciplinary Institute (EIIRIS), Director of Research Administration Center (RAC), Toyohashi University of Technology, Japan. He is now working as an Executive Counselor/Professor Emeritus, Toyohashi University of Technology, Japan.

Takeshi Kawano completed his M.S. in 2001 and Ph.D. in 2004 at the Department of Electrical and Electronic Engineering, Toyohashi University of Technology, Japan. From 2004–2005, he was a Postdoctoral Research Fellow at the same institution. From 2005–2007, he was a Postdoctoral Research Fellow (Japan Society for the Promotion of Science Postdoctoral fellowship for research abroad) in the Department of Mechanical Engineering, Berkeley Sensor and Actuator Center (BSAC), University of California, Berkeley, USA. From 2007–2010, he was an Assistant Professor, Department of Electrical and Electronic Engineering, Toyohashi University of Technology, Japan. Since 2010, he has been a PRESTO Researcher, Japan Science and Technology Agency (JST), as well as an Associate Professor, Department of Electrical and Electronic Information Engineering, Toyohashi University of Technology, Japan.